Electronic Supplementary Material (ESI) for Nanoscale.
This journal is © The Royal Society of Chemistry 2023

Supporting information

Charge Transport Transition of PEDOT:PSS Thin Film for Temperature-Insensitive Wearable Strain Sensors

Young Kyun Choi,[a] *Tae Hyuk Kim,*[b] *Jeong Han Song,*[c] *Byung Ku Jung,*[a] *Woosik Kim,*[a] *Jung Ho Bae,*[a] *Hyung Jin Choi,*[a] *Jeonghun Kwak,*[c]* *Jae Won Shim,*[b]* *and Soong Ju Oh*[a]*

[a] Department of Materials Science and Engineering, Korea University, Seoul 02841, Republic of Korea

[b] School of Electical Engineering, Korea University, Seoul 02841, Republic of Korea

[c] Department of Electrical and Computer Engineering, Inter-university Semiconductor Research Center, and Soft Foundry Institute, Seoul National University, Seoul 08826, Republic of Korea

*Corresponding author : sjoh1982@korea.ac.kr, jwshim19@korea.ac.kr, jkwak@snu.ac.kr

Discussion of GIWAXS measurment

For pristine and 5 vol% DMSO-doped PEDOT:PSS thin films, the grazing-incidence wide-angle x-ray scattering (GIWAXS) measurements were performed to investigate the crystallinity and π-π stacking distance (Fig. S5). The PEDOT:PSS thin film exhibits a specific GIWAXS diffraction pattern at $q = 1.2$ and 1.7 $Å^{-1}$ and the diffraction pattern for the 5 vol% DMSO sample is stronger than that for the pristine (Fig. S5 (a,b)), indicating that the DMSO doping improves the crystallinity of the PEDOT:PSS thin film. The peak intensities in the q_z direction are demonstrated in Fig. S5(c). A diffraction peak is observed near $q_z = 1.7$ $Å^{-1}$, which is attributed to the (010) face on π-π stacking between the PEDOT chains.[1,2] The q_z value shifts from 1.74 $Å^{-1}$ in pristine to 1.82 $Å^{-1}$ in 5 vol% DMSO, suggesting that the π–π stacking distance decreases with increasing DMSO doping owing to its relationship with the real space distance = $2\pi/q$. The calculated stacking distances are 3.61 and 3.45 Å for pristine and 5 vol% DMSO, respectively. Furthermore, electrical conductivity of the PEDOT:PSS thin film increases with DMSO secondary doping because of the reduced π-π stacking distance and improved crystallinity.

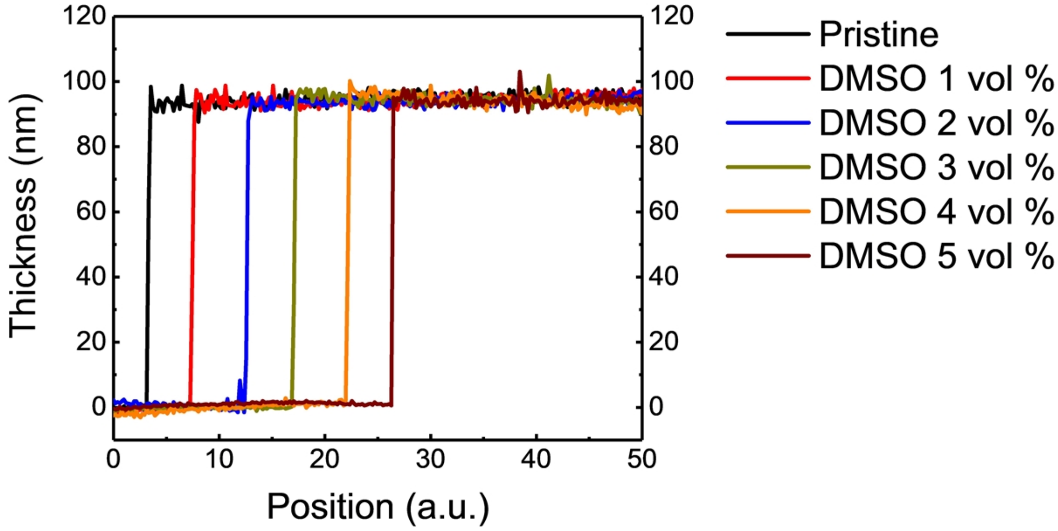

Figure S1. Thickness of the patterned PEDOT:PSS thin film measured by AFM.

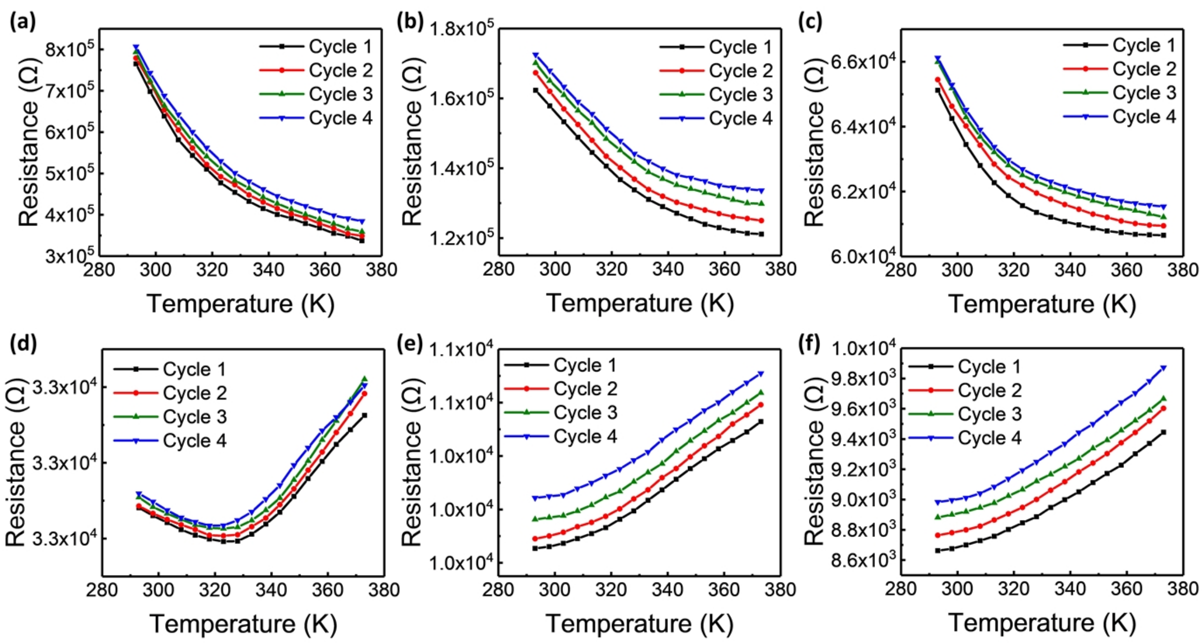

Figure S2. Temperature-dependent resistance change in 4-cycle tests of the prepared (a) pristine and (b) 1 vol%, (c) 2 vol%, (d) 3 vol%, (e) 4 vol%, and (f) 5 vol% DMSO-doped PEDOT:PSS thin films, respectively.

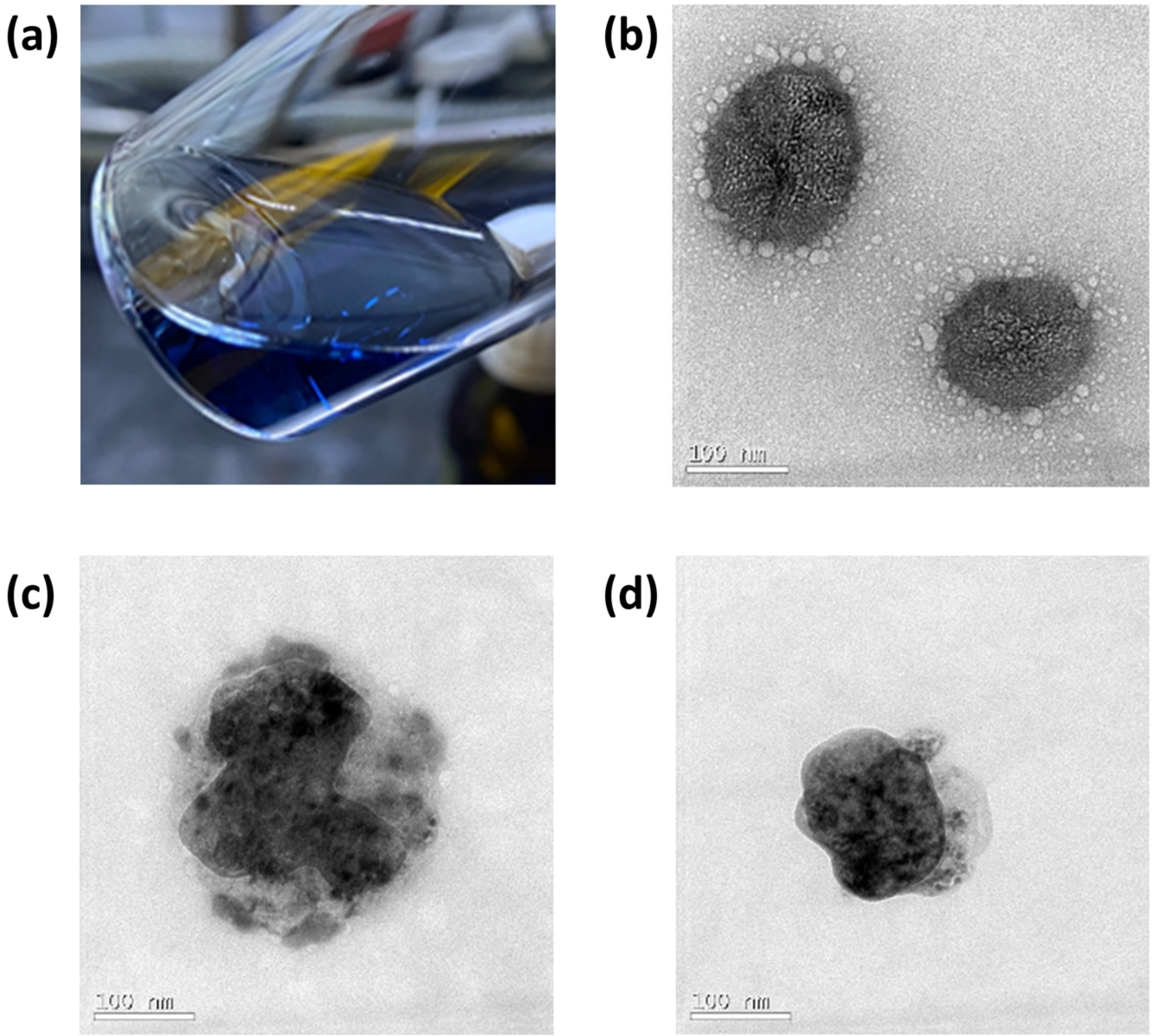

Figure S3. (a) Diluted PEDOT:PSS solution and TEM image of (b) pristine and (c) 3 vol%, (d) 5 vol% DMSO-doped PEDOT:PSS.

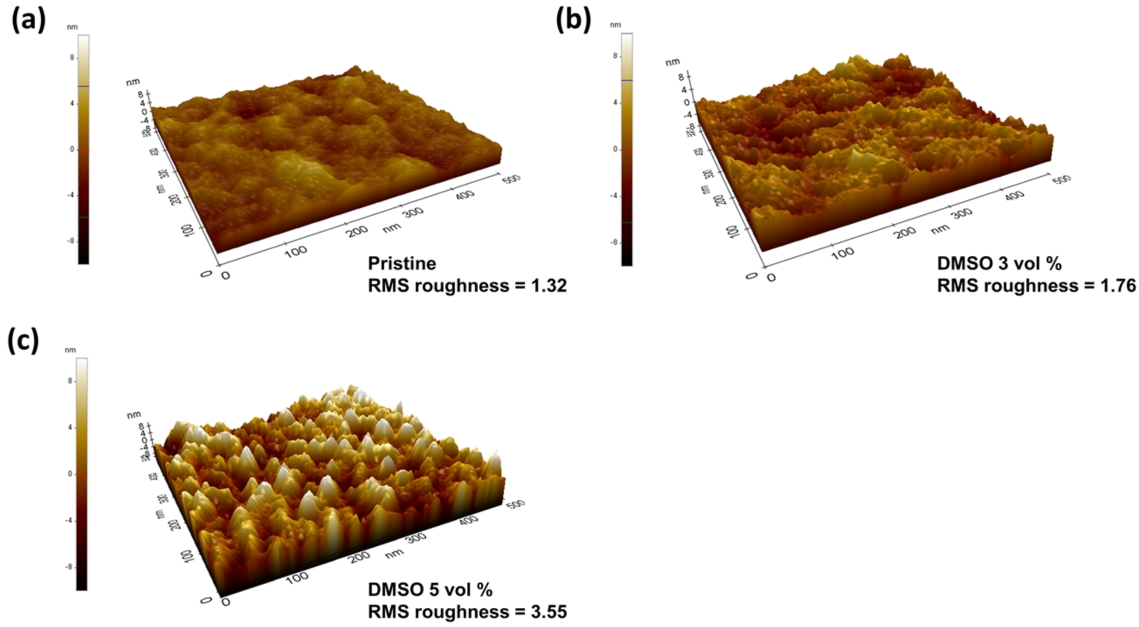

Figure S4. AFM 3D topography image (500 × 500 nm, 1024 pixel) and extracted RMS roughness of (a) pristine, (b) 3 vol%, and (c) 5 vol% DMSO-doped PEDOT:PSS thin film.

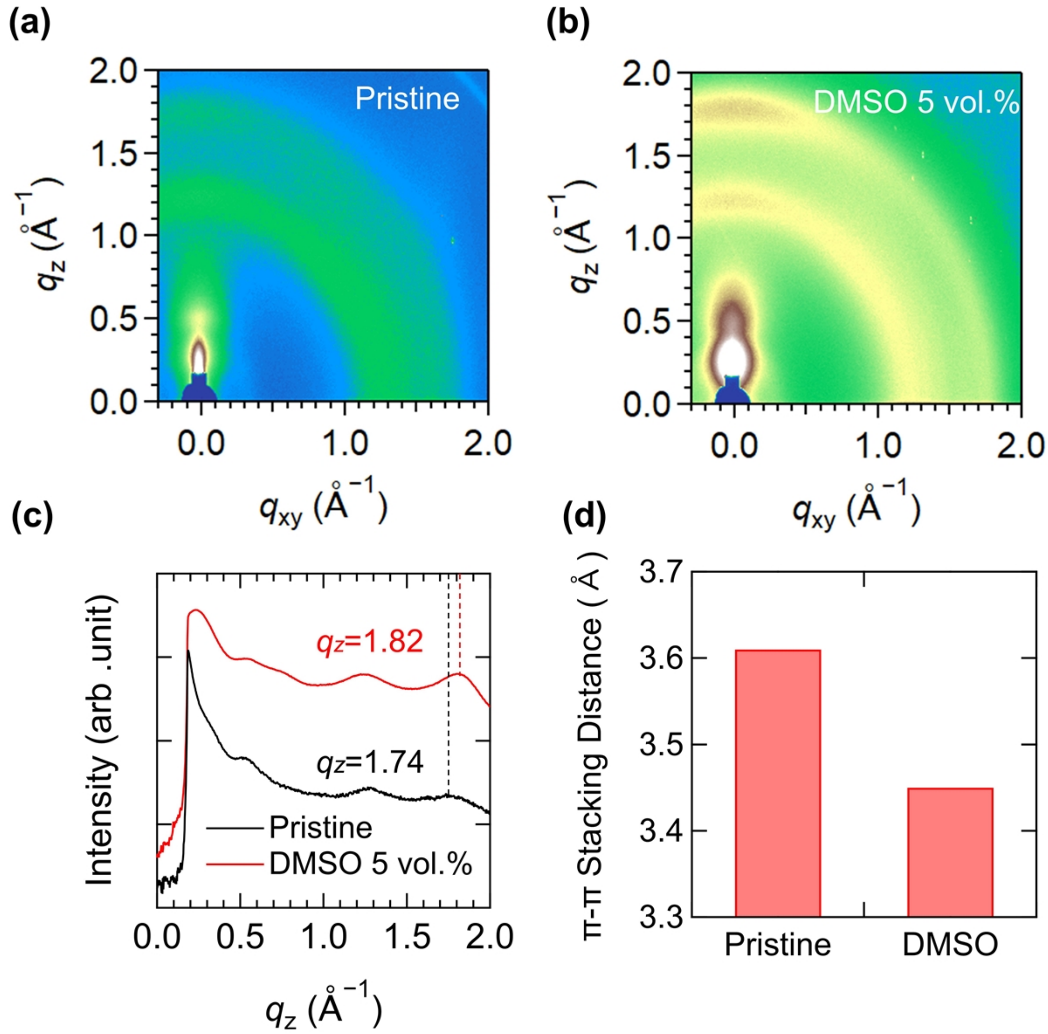

Figure S5. 2D GIWAXS pattern images of: (a) pristine and (b) 5 vol. % DMSO-doped PEDOT:PSS. (c) Corresponding vertical linecut (d) Calculated π-π stacking distance.

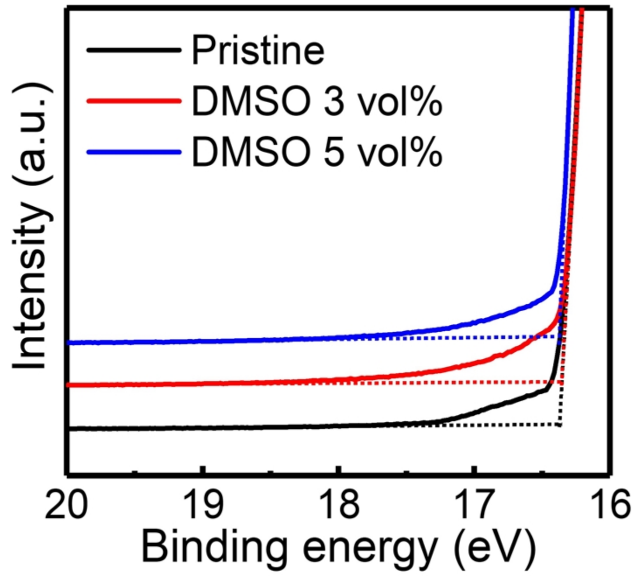

Figure S6. Secondary electron cut-off region of the UPS spectra (He I radiation) for pristine, 3 vol% DMSO, and 5 vol% DMSO PEDOT:PSS thin films.

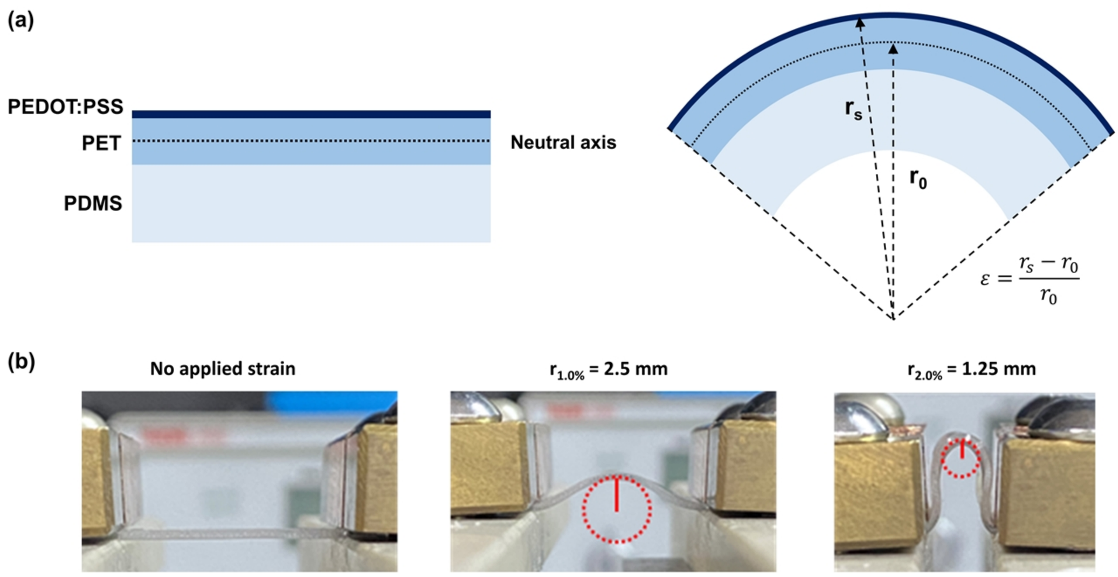

Figure S7. (a) Schematic of applied bending strain (b) Bending radius of 1.0 and 2.0 % bending strain.

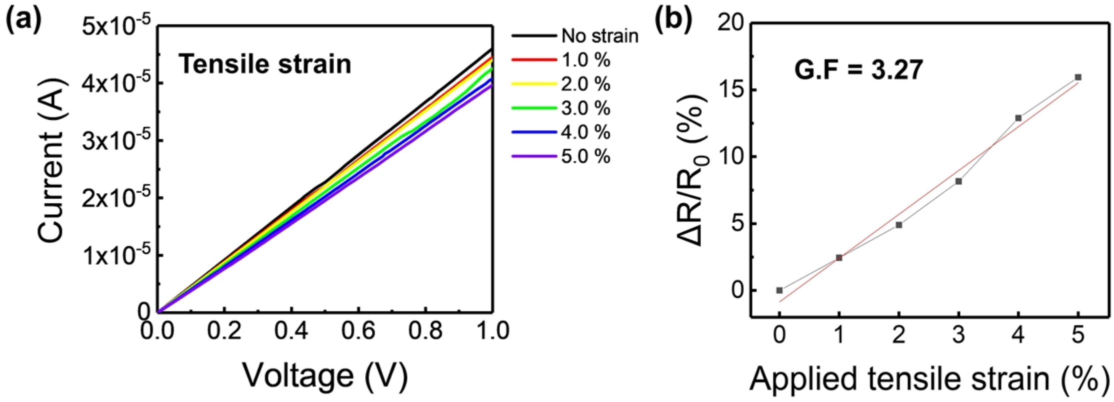

Figure S8. (a) Tensile strain response of 3 vol% DMSO-doped PEDOT:PSS thin-film strain sensor. (b) Relative resistance change ($\Delta R/R_0$) in response to the tensile strain. Even with applied tensile strain, the strain could be distinguished in 1 % interval and a obtained gauge factor similar to the bending strain.

Materials	**Application**	**TCR (/K)**	**Gauge factor**	**Seebeck coefficient (μV/K)**	**Reference**
PEDOT:PSS/CNT Composite	Strain sensor		4		(3)
PEDOT:PSS/SWCNT Composite	Stretchable electrode		21.5		(4)
PEDOT:PSS/CNF aerogels	Strain sensor		14.8		(5)
PU-PEDOT:PSS/SWCNT/PU-PEDOT:PSS	Strain sensor		62		(6)
Ag NWs/PEDOT:PSS/PU	Self-powered strain sensor		5~12		(7)
PEDOT:PSS/Ag NW	Strain sensor		3~8		(8)
PVA-PEDOT:PSS	Strain sensor		14		(9)
PVA-PEDOT:PSS nanofiber	Strain sensor		396		(10)
PEDOT:PSS-CNT composite	Strain sensor		150	35	(11)
PEDOT:PSS-NR composite	Stretchable and healable conductive elastomer		15	23	(12)
PEDOT:PSS/Ag NW/nylon thread	Strain sensor		1.69~3.31		(13)
PEDOT:PSS-Zonyl additive	Strain sensor		5.5		(14)
PEDOT:PSS-PDMS	Temperature sensor	4.2×10^{-2}			(15)
PEDOT:PSS-DMSO Monolayer	Temperature sensor	-2.5×10^{-3}			(16)
PEDOT:PSS-GOPS-CYTOP	Temperature sensor	-7.7×10^{-1}			(17)
PEDOT:PSS-DMSO monolayer	Anti-temperature interference strain sensor	-9.0×10^{-5}	2~3.3	16	This work

Table S1. Various PEDOT:PSS materials application with corresponding temperature coefficient of resistance, gauge factor and Seebeck coefficients.

Reference

1 C. M. Palumbiny, F. Liu, T. P. Russell, A. Hexemer, C. Wang and P. Müller-Buschbaum, *Adv. Mater.*, 2015, **27**, 3391–3397.

2 J. Dong and G. Portale, *Adv. Mater. Interfaces*, 2020, **7**, 18, 200641.

3 T. N. Lam, G. S. Lee, B. Kim, H. Dinh Xuan, D. Kim, S. Il Yoo and J. Yoon, Compos. *Sci. Technol.*, 2021, **210**, 108811.

4 P. Zhao, R. Zhang, Y. Tong, X. Zhao, T. Zhang, Q. Tang and Y. Liu, *ACS Appl. Mater. Interfaces*, 2020, **12**, 55083–55093.

5 J. Zhou and Y. Lo Hsieh, *ACS Appl. Mater. Interfaces*, 2018, **10**, 27902–27910.

6 E. Roh, B. Hwang, D. Kim, B. Kim and N. Lee, *ACS Nano*, 2015, **9**, 6252–6261.

7 B. U. Hwang, J. H. Lee, T. Q. Trung, E. Roh, D. Il Kim, S. W. Kim and N. E. Lee, *ACS Nano*, 2015, **9**, 8801–8810.

8 X. Fan, N. Wang, F. Yan, J. Wang, W. Song and Z. Ge, *Adv. Mater. Technol.*, 2018, **3**, 1800030.

9 X. Fan, N. Wang, J. Wang, B. Xu and F. Yan, *Mater. Chem. Front.*, 2018, **2**, 355–361.

10 N. Liu, G. Fang, J. Wan, H. Zhou, H. Long and X. Zhao, *J. Mater. Chem.*, 2011, **21**, 18962–18966.

11 X. He, J. Shi, Y. Hao, L. Wang, X. Qin and J. Yu, *Compos. Commun.*, 2021, **27**, 100822.

12 Y. Yang, G. Zhao, X. Cheng, H. Deng and Q. Fu, *ACS Appl. Mater. Interfaces*, 2021, **13**, 14599–14611.

13 J. Eom, J. S. Heo, M. Kim, J. H. Lee, S. K. Park and Y. H. Kim, *RSC Adv.*, 2017, **7**, 53373–53378.

14 S. Savagatrup, E. Chan, S. M. Renteria-Garcia, A. D. Printz, A. V. Zaretski, T. F. O'Connor, D. Rodriquez, E. Valle and D. J. Lipomi, *Adv. Funct. Mater.*, 2015, **25**, 427–436.

15 Y. Yu, S. Peng, P. Blanloeuil, S. Wu and C. H. Wang, *ACS Appl. Mater. Interfaces*, 2020, **12**, 36578–36588.

16 C. Bali, A. Brandlmaier, A. Ganster, O. Raab, J. Zapf and A. Hübler, *Mater. Today Proc.*, 2016, **3**, 739–745.

17 Y. F. Wang, T. Sekine, Y. Takeda, K. Yokosawa, H. Matsui, D. Kumaki, T. Shiba, T. Nishikawa and S. Tokito, *Sci. Rep.*, 2020, **10**, 2467.